

Article

Paleoenvironment Change and Organic Matter Accumulation of Marine Shale in the Zigong Area, Southern Sichuan Basin, China: A Case Study of Well Z303

Huimin Li ¹, Taohua He ^{1,2,*}  and Weifeng Li ¹

¹ Hubei Key Laboratory of Petroleum Geochemistry and Environment, Yangtze University, Wuhan 430100, China; 202071418@yangtzeu.edu.cn (H.L.); 19972805155@163.com (W.L.)

² School of Geosciences, China University of Petroleum (East China), Qingdao 266580, China

* Correspondence: hetaohua@yangtzeu.edu.cn

Abstract: Marine organic-rich shale is widely distributed in the Upper Ordovician Wufeng Formation (WF-F) and Silurian Longmaxi Formation (LMX-F), making it an important target for shale gas exploration and development. In order to clarify the paleoenvironment evolution characteristics and the effect of depositional environment on organic matter (OM) accumulation of the marine shale in the Wufeng and Longmaxi Formations, a series of geochemical and petrological experiments were carried out, including TOC, Rock-Eval pyrolysis, XRD, and major and trace element analyses. Research results show that based on the variation characteristics of TOC, mineral composition, and paleoenvironment evolution characteristics, four units can be identified from bottom to top: Wufeng Formation (WF-F), Lower Longmaxi Formation (L-LMX-F), Middle Longmaxi Formation (M-LMX-F) and Upper Longmaxi Formation (U-LMX-F). The high-quality marine shale developed in WF-F and LMX-F in the Zigong area (TOC: 0.65–4.56%, avg. 2.15%) contains type I kerogen (kerogen type index: 86.0–98.3, avg. 92.7) and OM in mature stage (average of R_b and T_{max} are 2.94%, 646 °C, respectively). Clay minerals (avg. 42.5%) and quartz (avg. 37.7%) dominate the mineral compositions, with subordinated dolomite (avg. 6.3%), feldspar (avg. 6.0%), calcite (avg. 4.0%), and pyrite (avg. 3.5%). Paleoenvironment indicators suggest that during the sedimentary period of WF-F and L-LMX-F, the paleoclimate condition was humid; the weathering condition, paleosalinity, and redox conditions were the strongest; and there was a relatively high level of paleoproductivity and a relatively low level of terrigenous detritus influx. However, during the period of M-LMX-F and U-LMX-F, the climate gradually changed from warm and humid to hot and dry; the intensity of weathering conditions, paleosalinity, and redox conditions was relatively reduced; terrigenous detritus influx increased; and the paleoproductivity decreased. Relationships between TOC and paleoclimate condition, paleosalinity, redox condition, paleoproductivity, and terrigenous detritus influx suggest that redox condition is most important controlling factor for OM enrichment. A combination of anoxic bottom water conditions and high primary productivity and a relatively low terrigenous input resulted in the enrichment of OM in the WF-F and L-LMX-F, making it a potential exploration and development target. The research can provide scientific guidance for the selection of potential shale gas development targets in the Zigong area.

Keywords: shale gas; Wufeng and Longmaxi Formations; paleoenvironment; organic matter enrichment mechanism; Zigong area; Sichuan Basin



Citation: Li, H.; He, T.; Li, W. Paleoenvironment Change and Organic Matter Accumulation of Marine Shale in the Zigong Area, Southern Sichuan Basin, China: A Case Study of Well Z303. *Energies* **2023**, *16*, 4015. <https://doi.org/10.3390/en16104015>

Academic Editor: Reza Rezaee

Received: 12 March 2023

Revised: 7 May 2023

Accepted: 8 May 2023

Published: 10 May 2023



Copyright: © 2023 by the authors. Licensee MDPI, Basel, Switzerland. This article is an open access article distributed under the terms and conditions of the Creative Commons Attribution (CC BY) license (<https://creativecommons.org/licenses/by/4.0/>).

1. Introduction

Due to the paleoclimate and relative sea level change, as well as strong volcanic activity, organic matter-rich black shale was widely developed worldwide during the Late Ordovician and Early Silurian periods [1–5]. With the development of horizontal well techniques and the wide application of large-scale hydraulic fracturing technologies, a

number of notable achievements have been made in the commercial exploitation of marine shale gas in the Sichuan Basin, China. There are now five national shale gas demonstration zones, namely Weiyuan, Changning, Fushun-Yongchuan, Fuling, and Beizhaotong.

Marine shale is relatively homogeneous compared with lacustrine shale [6]. Nevertheless, due to the effect of varied sedimentary environmental evolution, the composition and content of organic matter, mineralogy, and laminar structure of the Wufeng-Longmaxi shales exhibit extremely strong heterogeneity, which is important for the selection of shale gas production targets [3,7].

Extensive studies have emphasized the control of sedimentary environment organic matter (OM) enrichment in shale [8,9]. Generally, two main factors affect the enrichment of OM in shale: the source of OM and preservation conditions for OM. Paleoproductivity, paleoclimate, and volcanic activities all affect the source of OM, while redox environment, paleosalinity, and terrigenous detrital determine whether the organic matter can be effectively preserved [8,10,11]. Two models were proposed by Pedersen (1990) to explain the enrichment mechanism of OM: the preservation model and productivity model. The paleo-productivity model stresses the significance of high OM degradation rates as a means to generate an advantageous environment for OM accumulation, while the preservation model highlights that anoxic sedimentary environments provide better preservation conditions for the enrichment of OM [12]. However, it remains controversial which sedimentary environmental factors dominate the enrichment of organic matter.

There has been much research on shale gas potential, lithofacies, and micro-pore structure in the Sichuan Basin; studies on the sedimentary environment and OM accumulation are concentrated in the Jiaoshiba area in the Southeast Sichuan Basin, the Anyue area in the Central Sichuan Basin, and the Pengshui area in the Eastern Sichuan Basin. As a newly developed area, research on paleoenvironment change and OM accumulation in the Zigong area is insufficient, though it is crucial for the shale gas exploration and development this area. Thus, this study presents the X-ray diffraction (XRD), total organic carbon (TOC), and major/trace elements of marine shale samples collected from the Wufeng-Longmaxi Formations in Well Z303, Zigong Area, Southern Sichuan Basin, China. The objectives of this paper are to reconstruct the sedimentary environment characteristics of the marine shale in the study area, including paleoclimate, paleoredox conditions, paleoproductivity, paleosalinity, and terrigenous detrital input to clarify the main controlling factors for organic matter enrichment through correlation analysis of TOC and sedimentary environmental factors, which would provide reference for shale gas exploration in similar basins.

2. Geologic Setting

The region known as the Sichuan Basin can be found in the northern part of the Yangtze platform, South China (Figure 1A). In the period spanning from the Late Ordovician to the Early Silurian, the Yangtze platform underwent a gradual transformation into a semi-closed basin as a result of the collision between the Yangtze Block and the Cathaysia Block. Subsequently, the basin was covered by a widespread deposition of organic matter-rich black shale [13].

The study area is located in the Zigong area, Southern Sichuan Basin, China, in the middle of Weiyuan and Changning shale gas national demonstration zones (Figure 1B). The sampling well Z303 is located in the Huilongchang syncline (Figure 1C). The Upper Ordovician Wufeng Formation and Lower Silurian Longmaxi Formation in Well Z303 developed a set of high-quality black and gray-black shale, with a thickness of 105 m (Figure 2). XRD and TOC experiments were conducted on 105 samples. The mineral composition is mainly quartz and clay minerals, with an average content of 36.9% and 41.5%, respectively. The TOC content ranges from 0.65% to 5.75%, generally higher than 1%, with an average of 2.09%.

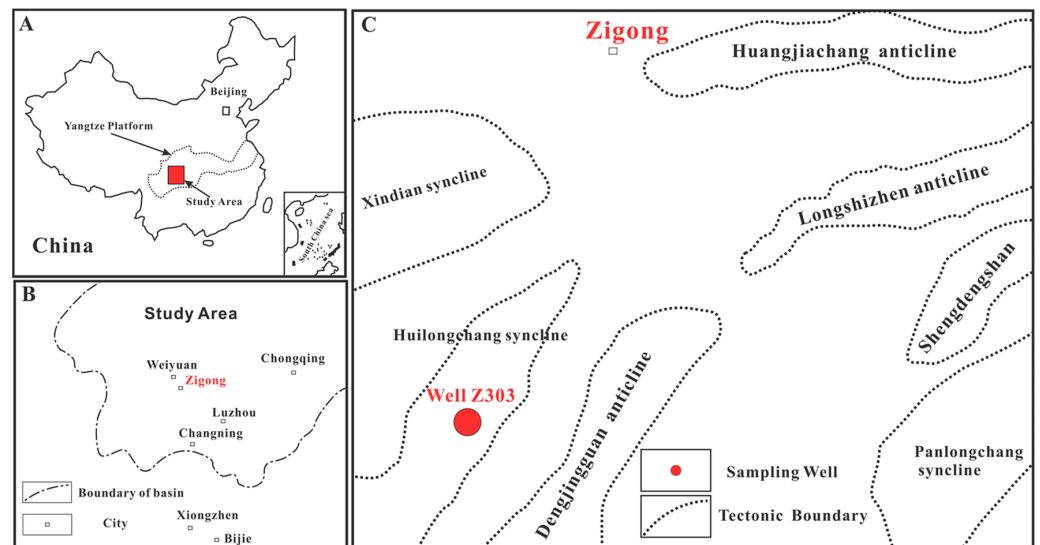


Figure 1. (A): Location of Yangtze Platform and Study Area in China; (B): Location of the study area in Southern Sichuan Basin; (C): Location of Well Z303 in Zigong Area.

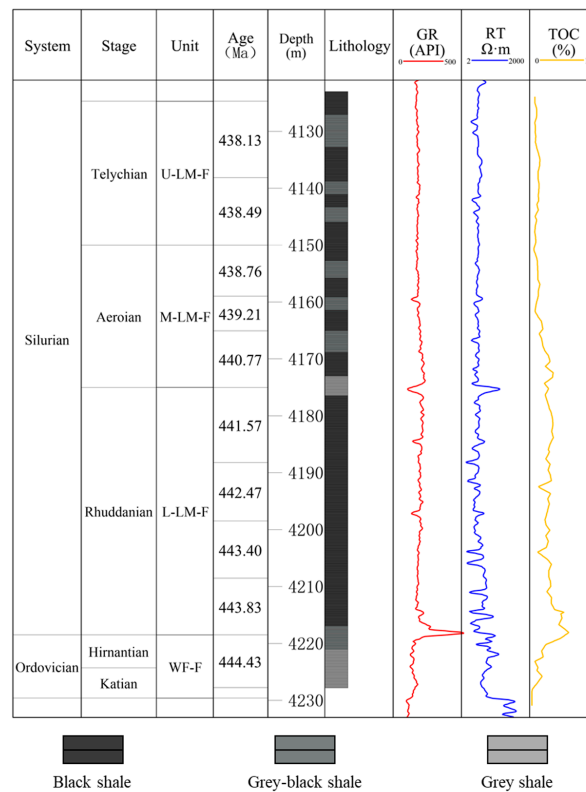


Figure 2. Stratigraphy, lithology and variations of GR, RT, and TOC in Well Z303; ages were obtained from [14].

3. Samples and Experiments Methods

3.1. Samples

In order to accurately describe the sedimentary environment and determine the organic matter enrichment mechanism, forty-nine samples were taken from Well Z303: forty-two samples from the Longmaxi Formation (LMX-F) and seven samples from the Wufeng Formation (WF-F). The sampling interval was between 0.68 and 2.85 m, with an average of 1.98 m. TOC, XRD, and major and trace element experiments were conducted for all the forty-nine samples.

3.2. Experimental Methods

3.2.1. XRD

An XRD examination was performed on the sample using a Rigaku D/max-rA X-ray diffractometer (Cu K α radiation, $\lambda = 0.15418$ nm, 40 kV, 100 mA) at a scan rate of $(2\theta)^\circ/\text{min}$ over the range of $3\text{--}70^\circ$. Mineral composition was determined semi-quantitatively from the area under the primary peak curve for each mineral. In order to identify the clay-mineral species, an XRD analysis was performed on the proportion of clay smaller than $2\ \mu\text{m}$.

3.2.2. TOC

All of the samples were given at least three washes using deionized water before they were examined, until the filtrate was clear. Following drying in an oven at $60\ ^\circ\text{C}$, samples (~ 0.10 g) were then pulverized in an agate mortar to a 200 mesh. After removing the inorganic carbon (carbonate and dolomite) using 10% HCl at $80\ ^\circ\text{C}$ for six hours in a crucible, we washed the shale samples using distilled water several times until the filtrate was neutral (pH ~ 7.0); thereafter, we were able to determine the TOC concentration by performing an analytical measurement using a LECO CS-600 carbon/sulfur analyzer.

3.2.3. Major and Trace Elements

For major elements, a Thermo Fisher ARL 9900 X-ray fluorescence spectrometer was used to identify major element concentrations at a detection limit greater than 0.01% after gravimetrically determining the loss on ignition (LOI) by heating the desiccated samples to $1100\ ^\circ\text{C}$ for 2 h. The scientific accuracy was typically greater than 3%.

For trace elements, we used an Aurora M90 inductively coupled plasma mass spectrometer (ICP-MS) with analytical accuracy of 5% to determine the trace element compositions and content. A HF-HNO₃ digestion process was carried out prior to the observations. (1) A Teflon container (10 mL) holding 50 mg of dry-ground samples was heated, and then 1.0 mL of HF on a hot plate was added at $120\ ^\circ\text{C}$ for the proper amount of time, resulting in the majority of Si being eliminated. (2) The extra sample in HF was disposed by first heating the vessel with 1.5 mL of HF and 2.0 mL of HNO₃ at $190\ ^\circ\text{C}$ for 72 h to fully dissolve the samples, and then heating it at $160\ ^\circ\text{C}$ for the proper period of time. (3) To prepare the sample before analysis, 1 mL of a 500 ng/mL internal Rh standard solution was added with enough deionized water to result in a 50 mL total amount.

3.2.4. Asphaltene Reflectance Values

A fluorescence microscope LABORLUX 12 POL microphotometer (MPV-3) was used to measure the asphaltene reflectance values (R_b) under a relatively stable temperature of $23 \pm 2\ ^\circ\text{C}$ during the experiment.

3.3. Data Analysis

The enrichment degree of the element X was determined in the form of enrichment factor (EF), according to the following equation:

$$X_{\text{EF}} = (X/\text{Al})_{\text{Sample}} / (X/\text{Al})_{\text{PAAS}}$$

where X and Al are the concentrations of an element X and Al, respectively. PAAS is the post-Achaean Australian shale [15].

Generally, $X_{\text{EF}} < 1$ represents a depleted concentration of an element X, whereas $X_{\text{EF}} > 1$ represents an enrichment element of an X relative to the PAAS concentrations.

4. Results

4.1. Organic Geochemical Characteristics

4.1.1. TOC Characteristics

The TOC concentrations of the shale samples in the study region are highly variable, ranging from 0.65% to 4.56%, with a mean value of 2.15%. This indicates that the study area

has a great potential for the production of hydrocarbons. The values of TOC of the shale samples from different units show great differences, with a decreasing trend from WF-F to the Upper Longmaxi Formation (U-LMX-F) (Figure 3). The TOC contents of the investigated shales in the WF-F, Lower Longmaxi Formation (L-LMX-F), Middle Longmaxi Formation (M-LMX-F), and U-LMX-F averaged 3.72%, 2.79%, 1.66%, and 1.06%, respectively. The TOC content of the investigated shale from the WF-F and L-LMX-F averaged 3.07%, which is more than twice that of the M-LMX-F and U-LMX-F (avg. 1.34%).

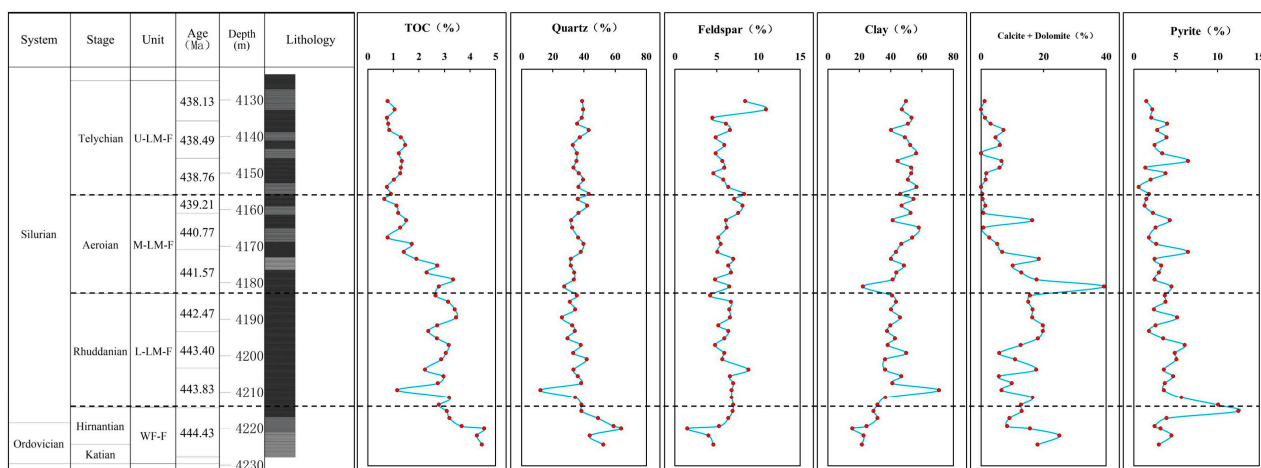


Figure 3. Variations of TOC and mineral composition in Well Z303.

4.1.2. Type of Organic Matter

The maceral content and composition of the eleven shale samples are shown in Table 1. The main type of maceral in the study area is sapropelinite (89–98%, avg. 95.7%), with a small amount of vitrinite (2–11%, avg. 4.3%). The type index of OM (TI) can be used to further differentiate OM type [16]. TI ranges from 80.8 to 96.5 (avg. 92.5), indicating all the shale samples belong to the type I Kerogen.

4.1.3. Maturity of Organic Matter

The asphaltene reflectance values (R_b) of the WF-F and LMX-F shale samples ranged from 3.0% to 3.5% and averaged 3.2%. The calculated vitrinite reflectance (R_{oc}) based on R_b ranged from 2.3% to 2.6%, with an average of 2.4%, indicating a late maturation period of OM. The T_{max} of the samples was in the range of 635 °C to 755 °C (avg. 670 °C), displaying a late maturation period of OM (Table 1).

Table 1. Information on the pyrolysis results and composition of organic macerals.

Sample ID	Depth (m)	Formation	Sapropelinite (%)	Vitrinite (%)	TI	Type	R_b (%)	R_{oc} (%)	T_{max} (°C)
Z303-7-①	4224.72	Wufeng	98	2	96.5	I	3.2	2.4	652
Z303-14-③	4218.07	Longmaxi	93	7	87.8	I	3.5	2.6	651
Z303-16-⑤	4215.52	Longmaxi	96	4	93.0	I	3.0	2.3	755
Z303-18-⑦	4214.52	Longmaxi	89	11	80.8	I	3.4	2.5	654
Z303-25-⑨	4208.225	Longmaxi	98	2	96.5	I	3.0	2.3	755
Z303-35	4198.245	Longmaxi	96	4	93.0	I	3.4	2.5	663
Z303-43	4189.525	Longmaxi	97	3	94.8	I	3.1	2.3	652
Z303-53-⑩	4179.395	Longmaxi	97	3	94.8	I	3.2	2.4	657
Z303-64	4168.505	Longmaxi	95	5	91.3	I	3.1	2.3	654
Z303-77-⑪	4154.86	Longmaxi	98	2	96.5	I	3.4	2.5	635
Z303-97-⑫	4136.06	Longmaxi	96	4	93.0	I	3.1	2.3	650

TI is the type index of OM, and $TI = (\text{sapropelinite} \times 100 + \text{lignite} \times 50 - \text{vitrinite} \times 75 - \text{inertinite} \times 100) / 100$ [16].

4.2. Mineral Composition and Lithofacies Classification

Clay minerals and quartz were found to be the most abundant minerals in the shale samples taken from the study area, according to the findings of mineral content and composition analyses (Figure 4A). The percentage of clay elements found was the greatest, ranging from 14.7% to 71.0% (with an average of 42.5%), followed by the percentage of quartz, which ranged from 12.0% to 78.0% (with an average of 37.7%). The average content of the other minerals was no more than 10%: dolomite (avg. 6.3%), feldspar (avg. 6.0%), calcite (avg. 4.0%), and pyrite (avg. 3.5%). The percentage of brittle minerals, which includes quartz, dolomite, and calcite, makes up 48.0% of the total. The predominant component of clay minerals was a mixed layer of illite and smectite, which had a relative average content of 54.9%. This was followed by illite and chlorite, each of which had a relative average content of 21.7% and 18.8%, respectively. Finally, the chlorite-smectite mixed layer had a relative average content of 4.6% (Figure 4B).

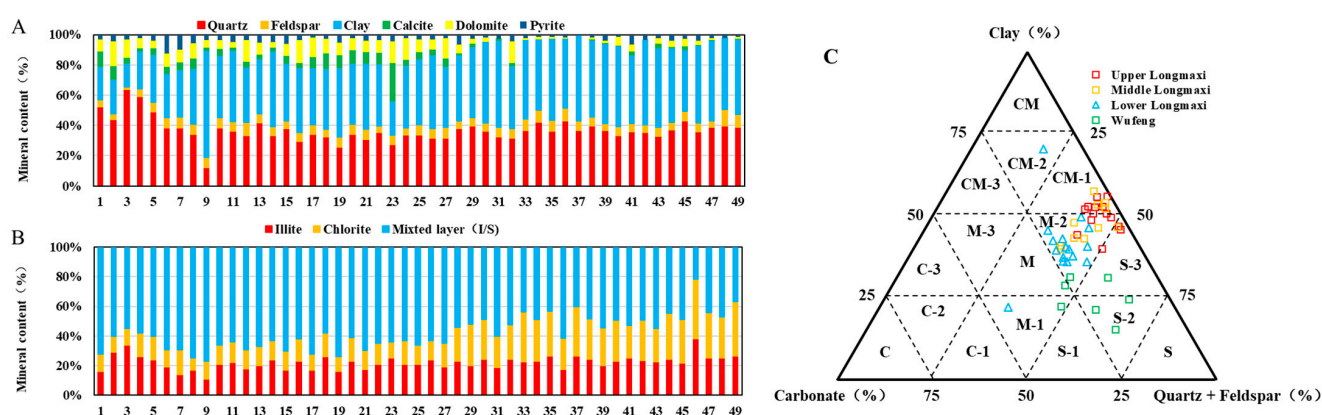


Figure 4. Mineral composition and lithofacies classification of the Wufeng and Longmaxi shales. (A), mineral composition; (B), clay mineral composition; (C), lithofacies classification, modified after [17]. S: siliceous shale lithofacies; S-1: carbonate-rich siliceous shale lithofacies; S-2: mixed siliceous shale lithofacies; S-3: clay-rich siliceous shale lithofacies; m: Mixed shale lithofacies; M-1: calcareous/siliceous mixed shale lithofacies; M-2: argillaceous/siliceous mixed shale lithofacies; M-3: argillaceous/calcareous mixed shale lithofacies; CM: argillaceous shale lithofacies; CM-1: silica-rich argillaceous shale lithofacies; CM-2: mixed argillaceous shale lithofacies; CM-3: carbonate-rich argillaceous shale lithofacies.

The lithofacies classification scheme in this paper was proposed by Wu et al. [17]. According to their method, the end members of the lithofacies classification ternary graph are carbonate minerals, silicon minerals, and clay minerals. The shale samples were divided into sixteen types. The distribution of the forty-nine marine shale samples from the study area is illustrated in Figure 4C. These samples are broken up into a total of eight different lithofacies zones. These zones are labeled as follows: argillaceous/siliceous mixed shale lithofacies (M-2), calcareous/siliceous mixed shale lithofacies (M-1), mixed shale lithofacies (M), mixed argillaceous shale lithofacies (CM-2), silica-rich argillaceous shale lithofacies (CM-1), clay-rich siliceous shale lithofacies (S-3), mixed siliceous shale lithofacies (S-2), and siliceous shale lithofacies (S).

4.3. Major and Trace Elements

Table 2 presents the results of the major and trace element investigations performed on the shale samples obtained from the Wufeng and Longmaxi Formations.

Table 2. Major and trace element concentrations in Well Z303.

Sample ID	Major Elements, %												Trace Elements, ppm									
	SiO ₂	Al ₂ O ₃	CaO	K ₂ O	FeO	MgO	Fe ₂ O ₃	Na ₂ O	TiO ₂	P ₂ O ₅	MnO	Ba	V	Sr	Zn	B	Cr	Ni	Cu	Mo	Co	U
Z303-13	64.81	6.33	9.17	1.54	0.70	1.36	1.50	0.54	0.41	0.142	0.035	1555	275	192	327	54.3	50.8	137	125	24.4	7.83	6.6
Z303-15-④	60.64	7.50	9.24	1.87	0.84	1.92	2.27	0.48	0.40	0.120	0.048	2018	165	207	80.5	50.8	40.9	110	65.7	65.1	13.8	28.1
Z303-17-⑥	74.80	4.91	4.87	1.30	0.86	1.28	1.29	0.30	0.26	0.067	0.038	1666	182	104	210	51	33.5	89.1	40.4	38.5	7.45	12.7
Z303-19-⑧	74.71	7.27	2.98	1.82	1.26	1.37	1.41	0.52	0.40	0.082	0.027	2002	112	88.4	130	67.5	41	61.4	41.2	18.2	9.27	7.36
Z303-21	68.64	9.74	4.13	2.35	1.60	1.81	2.16	0.67	0.52	0.088	0.033	2430	120	118	92.4	97	53.8	65.8	46.4	20.8	12	6.8
Z303-23	61.46	10.75	4.37	2.45	1.66	2.16	5.29	0.75	0.58	0.104	0.037	1146	109	113	66.1	77.5	62.6	70.3	55	22.4	13.3	8.27
Z303-25-⑩	59.02	11.52	5.19	2.60	1.70	2.36	4.99	0.83	0.62	0.106	0.040	1316	106	124	63.6	93.8	61.1	68.8	54.3	25.9	14.1	7.6
Z303-27	53.17	13.21	7.96	3.06	2.00	3.09	2.94	0.89	0.62	0.089	0.058	2661	82.4	165	43.5	89.4	60.3	37.9	63.4	23	15.4	7.79
Z303-29	49.86	26.04	1.84	6.02	2.08	3.15	2.32	1.16	0.62	0.120	0.026	4904	75	147	63.6	272	30	26.7	22.3	13.9	8.84	7.02
Z303-31	59.92	13.44	5.07	3.17	2.22	2.71	1.97	0.87	0.64	0.089	0.038	2718	129	140	100	94.7	65.1	70	49.8	19	13.5	7.26
Z303-33	58.51	15.37	2.94	3.79	2.38	2.79	2.46	0.95	0.70	0.108	0.031	3260	139	126	75.7	147	73	54.9	64.1	21.3	17.2	9.12
Z303-35	56.20	15.12	5.09	3.62	2.42	3.24	2.34	0.89	0.74	0.102	0.051	5121	132	169	76.4	110	64.2	70.7	55.9	18.4	15	7.9
Z303-37	56.51	15.27	4.33	3.91	2.22	3.06	2.70	0.78	0.64	0.100	0.038	3430	172	138	88.1	124	76.3	91.2	73.3	21.1	16.5	10.4
Z303-39	58.84	15.65	2.76	3.95	2.38	2.89	3.09	0.84	0.68	0.112	0.028	2719	141	125	77.9	113	80	65.1	70.6	23.3	18	11.9
Z303-41	58.47	13.57	4.32	3.41	2.50	2.65	2.79	0.72	0.61	0.100	0.036	2051	128	131	68.6	108	68.5	69.4	62.1	24.2	16.4	10.9
Z303-43	50.45	15.40	6.19	3.82	3.10	3.92	2.17	0.81	0.62	0.104	0.062	3262	162	162	98.6	98.8	72.1	72.8	50.3	13.5	15.7	6.58
Z303-45	49.34	13.77	8.36	3.43	2.78	3.47	1.51	0.71	0.59	0.087	0.067	3287	202	179	134	87.9	65.2	73.2	47.1	16.3	12.7	6.13
Z303-47	50.08	14.91	8.38	3.65	2.66	3.25	1.91	0.78	0.65	0.102	0.053	3260	195	185	128	98.7	70.4	88.6	50.9	23	14.8	10.4
Z303-49	48.66	16.94	7.08	4.13	2.65	3.54	2.74	0.92	0.70	0.120	0.043	2804	127	176	55.2	117	73	61.5	68	26.8	19.6	12.4
Z303-51	50.48	17.09	6.07	4.22	2.33	3.24	2.39	0.99	0.78	0.121	0.037	4162	201	169	102	148	78.5	101	70.1	30.2	18.8	14.1
Z303-53-⑩	50.82	17.81	5.88	4.33	2.52	3.22	2.59	1.00	0.78	0.133	0.037	3815	188	164	126	140	72.1	99.4	64	33.9	17.1	12
Z303-55	50.79	16.40	7.79	3.89	2.64	3.17	1.64	1.01	0.83	0.132	0.044	6743	157	185	85	110	73.2	81.6	53.9	21.1	16	8.8
Z303-57	40.02	13.57	15.28	3.01	2.28	3.51	2.11	0.95	0.69	0.204	0.066	2985	71.1	312	52	97.3	52.8	32.3	54.9	9.15	10.7	3.47
Z303-59	51.22	15.79	5.95	3.98	2.98	3.63	2.04	0.83	0.67	0.120	0.059	3645	490	153	211	117	80.2	112	61	25.6	14	11.8
Z303-61	52.90	15.71	5.68	3.96	2.70	3.21	2.35	0.84	0.67	0.113	0.049	3608	465	145	147	112	78.5	108	60.6	21.1	14.9	11.3
Z303-63	56.48	16.53	3.72	4.27	2.52	3.03	2.29	0.95	0.73	0.112	0.043	5096	331	131	141	123	85.1	98.2	57.7	22.9	15.3	13.9
Z303-65	50.38	16.80	6.46	4.16	2.74	3.70	2.47	0.93	0.68	0.113	0.094	4930	293	165	131	103	78	78.6	50.6	16.1	13	9
Z303-67	58.82	16.27	2.59	4.16	3.26	3.13	2.63	0.84	0.60	0.093	0.053	3283	255	112	134	121	83.9	80.1	54.5	11.1	15.8	8.2
Z303-69	57.08	16.62	2.45	4.30	3.64	3.29	2.47	0.83	0.58	0.094	0.065	3095	261	105	115	107	87.2	76.3	60.5	10.4	16.1	8.74
Z303-71	60.95	17.46	0.86	4.44	4.20	3.43	2.27	0.90	0.60	0.107	0.051	3281	169	90.3	136	130	91.4	62.1	44	5.03	18.8	4.97
Z303-73	57.72	18.34	1.41	4.78	4.08	3.45	2.12	0.95	0.61	0.095	0.052	3344	191	106	127	125	95.6	65.8	81.5	7.92	16.5	4.72
Z303-75	51.43	17.48	3.97	4.23	4.07	3.92	3.07	0.96	0.57	0.092	0.148	3000	195	133	115	109	87.3	76.3	59.6	8.95	18.3	3.9
Z303-77-⑩	61.63	17.72	0.57	4.49	4.60	3.33	1.81	1.06	0.58	0.084	0.050	3022	178	82.7	128	141	95.4	60.5	50.4	7.08	17.6	3.47
Z303-79	60.54	17.53	0.68	4.41	4.32	3.38	2.08	1.01	0.59	0.088	0.058	3103	171	82.6	73.7	106	92.3	55.2	34	3.62	16.6	3.44
Z303-81	60.43	17.72	0.65	4.46	4.46	3.48	2.18	1.01	0.61	0.089	0.059	2962	178	82.2	109	128	95.8	56.4	52.4	3.69	17.8	3.16
Z303-83	60.38	17.35	0.76	4.37	4.86	3.39	1.60	1.01	0.61	0.090	0.064	2832	220	83.8	191	122	94.1	60	51.6	7.3	17.3	3.91
Z303-85	60.36	17.54	0.41	4.45	4.52	3.37	2.08	0.99	0.58	0.091	0.052	2913	174	74.8	94.4	112	93.8	60	42.1	4.07	17.8	2.83
Z303-87	60.18	17.96	0.78	4.50	4.43	3.46	2.14	1.03	0.65	0.097	0.054	3608	203	87.4	130	139	93.8	65.3	73.6	8.5	18.4	3.77
Z303-89	58.83	18.15	1.08	4.63	3.74	3.43	3.10	1.03	0.59	0.086	0.059	3054	205	87.8	95.6	135	93.1	71.6	58.1	9.12	18.3	3.87
Z303-91	58.19	17.59	1.53	4.42	4.10	3.26	2.19	1.16	0.59	0.085	0.068	2898	246	95	200	106	93.3	74.4	55.2	10.6	17.1	3.93
Z303-93	56.58	17.68	2.18	4.42	3.46	3.27	3.16	1.11	0.64	0.088	0.080	3753	175	111	113	128	89.4	76.3	57	10.6	16.9	5.81
Z303-95	58.08	17.82	0.85	4.53	3.68	3.24	3.16	1.07	0.57	0.089	0.050	3000	155	83	87.8	113	92.6	66.7	52.3	9.2	17.8	4.86
Z303-97-⑩	56.35	17.83	2.57	4.45	3.56	3.17	2.69	1.18	0.64	0.087	0.069	2939	133	114	125	106	77.4	70.9	53.4	13.7	17.1	7.49
Z303-99	59.48	17.59	1.21	4.39	3.82	3.13	2.84	1.16	0.57	0.089	0.057	2877	147	89.3	142	152	89.2	77.6	78	12.9	20.2	4.64
Z303-101	60.16	14.77	3.71	3.64	3.90	2.94	1.94	0.94	0.50	0.075	0.144	2533	111	120	89.2	99.5	75.2	45.3	42.4	7.16	14.6	2.83
Z303-103	58.80	17.84	1.17	4.47	4.28	3.40	2.70	1.06	0.56	0.089	0.070	2812	145	90.1	94.4	106	94.9	65	50.5	7.39	18.2	3.41
Z303-105	59.54	18.12	0.85	4.66	4.48	3.36	2.06	1.06	0.56	0.092	0.058	2921	138	86.8	104	123	92.1	53	66.1	5.42	19.2	2.91
Z303-107	60.02	17.98	0.59	4.48	5.32	3.28	1.26	1.24	0.57	0.090	0.053	2741	148	74.7	115	104	95.2	58	52.5	6.18	17.5	3.48
Z303-109	59.62	18.28	0.54	4.65	5.06	3.34	1.52	1.16	0.58	0.093	0.054	2657	142	74.6	109	105	97.2	54.2	46.5	5.11	18.8	2.17

SiO₂ is the dominant constituent, followed by Al₂O₃, and a small amount of CaO, K₂O, FeO, MgO, Fe₂O₃, Na₂O, TiO₂, P₂O₅, and MnO. The concentration of SiO₂ and Al₂O₃ range from 40.02% to 74.80% (avg. 57.39%) and 4.91% to 26.04% (avg. 15.55%), respectively. The average concentration of major elements, including CaO, K₂O, FeO, MgO, and Fe₂O₃, is below 5%, and the mean concentrations of Na₂O, TiO₂, P₂O₅, and MnO is no more than 1%.

The most abundant trace element is Ba (avg. 3126.98 ppm), followed by V (181.42 ppm), Sr (avg. 128.15 ppm), Zn (avg. 114.33 ppm), B (avg. 112.66 ppm), Cr (avg. 65.9 ppm), Ni (avg. 71.97 ppm), and Cu (avg. 57.04 ppm); the concentration of other elements such as Mo, Co and U were less than 30 ppm.

5. Discussion

5.1. Depositional Environment Analysis

5.1.1. Paleoclimate and Weathering Conditions

The content and ratios of specific trace elements can indicate the characteristics of the sedimentary environment. The Sr/Cu ratio is considered to be a useful indicator of paleoclimate, since Sr is concentrated under arid conditions, and Cu is enriched under humid conditions [18]. Sr/Cu < 5, 5 < Sr/Cu < 10, and Sr/Cu > 10 indicate humid, semiarid to semihumid, and arid climatic conditions, respectively [19]. The Sr/Cu ratio of the investigated shale samples from WF-F, L-LMX-F, M-LMX-F, and U-LMX-F average 6.62, 5.01, 1.98, and 1.68, respectively (Table 3). This shows that during the period of WF-F and L-LMX-F, the paleoclimate is semiarid to semihumid, becoming humid during the period of M-LMX-F and U-LMX-F in Well Z303 (Figure 5).

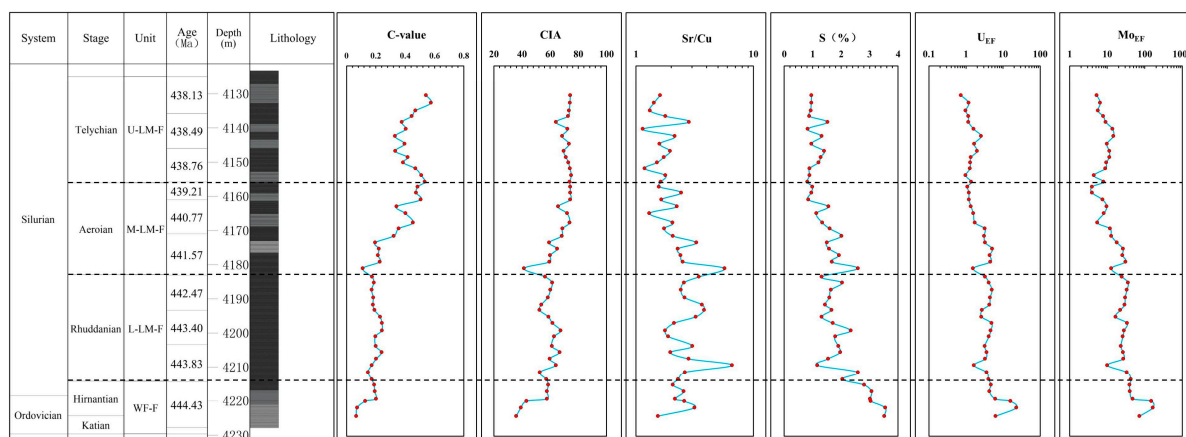


Figure 5. Variations of TOC, C-value, CIA, S, U_{EF}, and Mo_{EF} in Well Z303.

When the paleoclimate circumstances become hot and dry, K, Na, Sr, Ba, Ca, and Mg are more concentrated; this has been demonstrated by a significant number of studies. Elements such as V, Cr, Ni, Co, Fe, and Mn are comparatively enhanced under humid and wet conditions. Thus, C-value ($\Sigma(V + Co + Ni + Cr + Fe + Mn) / \Sigma(K + Ba + Sr + Na + Ca + Mg)$) has seen widespread use in determining the ancient environment preserved in shale sediments [20–22]. Generally, C-values < 0.2, 0.2 < C-values < 0.8, and C-values > 0.8 indicate arid, arid–humid and humid paleoclimate conditions, respectively. The C-value of the investigated shale samples from WF-F, L-LMX-F, M-LMX-F, and U-LMX-F average 0.15, 0.19, 0.35, and 4.4, respectively (Table 3). The paleoclimate is hot and arid in WF-F and L-LMX-F, changing to relatively humid paleoclimate conditions during M-LMX-F and U-LMX-F period in Well Z303 (Figure 5).

Table 3. TOC and trace element ratios in Well Z303.

Sample ID	Depth	TOC	Sr/Cu	C-Value	CIA	S	U _{EF}	Mo _{EF}	Cu/Ti	P/Ti	Al ₂ O ₃	Unit
Z303-13	4219.12	4.47	8.58	0.07	80.99	3.52	6.35	72.81	508.13	0.29	6.33	WF-F
Z303-15-④	4216.65	4.27	8.15	0.07	42.45	3.55	22.83	163.96	273.75	0.25	7.50	
Z303-17-⑥	4214.74	4.56	7.57	0.13	73.79	3.04	15.76	148.11	258.97	0.22	4.91	
Z303-19-⑧	4214.06	3.67	5.15	0.20	67.94	3.02	6.17	47.29	171.67	0.17	7.27	
Z303-21	4211.895	3.20	6.54	0.19	54.50	3.07	4.25	40.34	148.72	0.14	9.74	
Z303-23	4209.955	3.09	5.05	0.19	43.16	2.81	4.69	39.36	158.05	0.15	10.75	
Z303-25-⑩	4208.225	2.79	5.28	0.17	41.60	2.04	4.02	42.47	145.97	0.14	11.52	
Z303-27	4206.065	3.19	6.60	0.15	33.62	2.59	3.59	32.89	170.43	0.12	13.21	L-LM
Z303-29	4203.935	1.16	6.59	0.17	55.74	1.16	1.64	10.08	59.95	0.16	16.04	
Z303-31	4202.035	2.75	2.81	0.20	53.50	1.54	3.29	26.7	129.69	0.12	13.44	
Z303-33	4200.105	2.96	3.97	0.24	44.02	1.97	3.62	26.18	152.62	0.13	15.37	
Z303-35	4198.245	2.24	3.02	0.20	47.15	1.90	3.18	22.99	125.90	0.12	15.12	
Z303-37	4195.405	2.88	4.88	0.20	47.02	1.79	4.15	26.1	190.89	0.13	15.27	
Z303-39	4193.645	3.05	3.77	0.24	42.58	2.34	4.63	28.12	173.04	0.14	15.65	
Z303-41	4191.425	3.17	3.11	0.24	41.98	1.71	4.89	33.69	169.67	0.14	13.57	
Z303-43	4189.525	2.71	3.22	0.23	52.61	1.32	2.6	16.56	135.22	0.14	15.40	
Z303-45	4187.545	2.37	5.80	0.19	61.10	1.66	2.71	22.36	133.05	0.12	13.77	
Z303-47	4185.945	2.72	5.63	0.18	56.88	1.44	4.25	29.14	130.51	0.13	14.91	
Z303-49	4183.805	3.46	5.59	0.18	35.03	1.59	4.46	29.88	161.90	0.14	16.94	
Z303-51	4181.585	3.41	5.41	0.17	47.86	1.64	5.03	33.38	149.79	0.13	17.09	
Z303-53-⑩	4179.395	3.14	6.56	0.19	53.72	2.03	4.11	35.95	136.75	0.14	17.81	
Z303-55	4177.695	2.66	5.43	0.17	46.52	1.31	3.27	24.3	108.23	0.13	16.40	
Z303-57	4175.205	2.78	7.68	0.11	43.47	2.59	1.56	12.74	132.61	0.25	13.57	
Z303-59	4173.255	3.34	2.51	0.23	66.08	1.67	4.55	30.62	151.74	0.15	15.79	M-LM
Z303-61	4171.305	2.30	2.39	0.21	59.04	1.92	4.38	25.37	150.75	0.14	15.71	
Z303-63	4169.365	2.72	2.27	0.22	56.11	1.58	5.12	26.17	131.74	0.13	16.53	
Z303-65	4167.565	1.91	3.26	0.20	57.37	1.50	3.26	18.1	124.02	0.14	16.80	
Z303-67	4165.575	1.41	2.06	0.32	57.99	2.01	3.07	12.89	151.39	0.13	16.27	
Z303-69	4163.415	1.73	1.74	0.36	53.65	1.60	3.2	11.82	173.85	0.14	16.62	
Z303-71	4161.635	0.78	1.25	0.45	58.00	1.34	1.73	5.44	122.22	0.15	17.46	
Z303-73	4158.91	1.27	1.30	0.40	54.78	1.13	1.57	8.16	222.68	0.13	18.34	
Z303-75	4156.88	1.50	2.23	0.34	53.87	1.55	1.36	9.67	174.27	0.14	17.48	
Z303-77-⑩	4154.86	1.20	1.64	0.51	55.14	0.85	1.19	7.55	144.83	0.12	17.72	
Z303-79	4152.77	1.13	1.59	0.47	42.84	0.95	1.2	3.9	96.05	0.13	17.53	
Z303-81	4151	0.65	1.57	0.49	51.89	0.99	1.09	3.93	143.17	0.12	17.72	
Z303-83	4149.56	0.91	1.62	0.53	64.96	0.81	1.37	7.95	140.98	0.13	17.35	U-LM
Z303-85	4147.66	0.75	1.78	0.51	48.65	0.89	0.98	4.38	120.98	0.13	17.54	
Z303-87	4145.63	1.02	1.19	0.47	55.68	0.89	1.28	8.94	188.72	0.13	17.96	
Z303-89	4143.83	1.27	1.51	0.39	47.96	1.21	1.3	9.49	164.12	0.12	18.15	
Z303-91	4142.26	1.30	1.72	0.42	65.44	1.28	1.36	11.38	155.93	0.12	17.59	
Z303-93	4140.43	1.34	1.95	0.33	52.57	1.40	2	11.32	148.44	0.12	17.68	
Z303-95	4138.29	1.22	1.59	0.40	45.92	0.96	1.66	9.75	152.92	0.13	17.82	
Z303-97-⑩	4136.06	1.46	2.13	0.33	57.28	1.31	2.56	14.51	139.06	0.11	17.83	
Z303-99	4133.93	1.30	1.14	0.40	57.90	0.82	1.61	13.85	228.07	0.13	17.59	
Z303-101	4131.88	0.84	2.83	0.38	51.15	1.52	1.17	9.16	141.33	0.13	14.77	
Z303-103	4130.13	0.81	1.78	0.45	47.56	0.88	1.16	7.82	150.30	0.13	17.84	
Z303-105	4128.5	0.76	1.31	0.47	51.27	0.93	0.98	5.65	196.73	0.14	18.12	
Z303-107	4126.17	1.05	1.42	0.58	52.80	0.95	1.18	6.49	153.51	0.13	17.98	
Z303-109	4123.91	0.78	1.60	0.54	51.19	0.96	0.72	5.28	133.62	0.14	18.28	

It is worth noting that there is an obvious difference in results of the characterization of paleoclimate using the two parameters. However, C-values and Sr/Cu display good negative correlation ($R^2 = 0.83$), which indicates C-values can be used to characterize paleoclimate conditions (Figure 6).

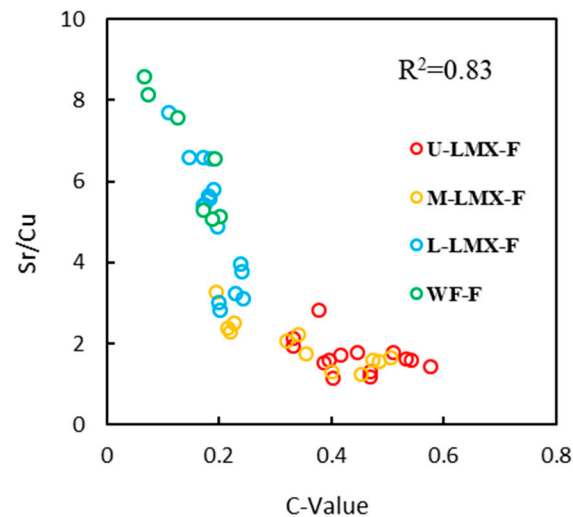


Figure 6. Correlations between Sr and C-value in Well Z303.

The chemical indicator of modification (CIA) is used by many researchers as a method for estimating the intensity of chemical environmental conditions [23,24]. Generally, $CIA < 70$, $70 < CIA < 80$, and $CIA > 80$ reflect weak, medium, and strong chemical weathering conditions, respectively. CIA values range from 36.01–74.99 (avg. 63.51), displaying weak to medium weathering conditions during the overall Wufeng and Longmaxi Formations. The CIA profile exhibits a long-term increase upward, with the average CIA values in the four units being 49.96, 58.66, 67.89, and 72.08, respectively (Table 3, Figure 5).

5.1.2. Paleosalinity

Paleosalinity is one of the most important factors controlling the circumstances under which organic matter can be preserved [25–27]. S (sulfur) is commonly used to characterize the salinity of water. Studies demonstrate that $S < 0.5$, $0.5 < S < 2$, and $Sr/Ba > 2$ indicate fresh water, brackish water, and saline water environments, respectively [28].

Statistical results show that the S ratios of the study area are in the range of 0.81–3.55, with an average of 1.68, indicating a brackish and saline water condition. The average S ratio in WF-F, L-LMX-F, M-LMX-F, and U-LMX-F is 3.01, 1.79, 1.42, and 1.05, respectively, indicating the salinity of water gradually decreases from bottom to top in Well Z303 (Table 3, Figure 5).

5.1.3. Redox Conditions

Some trace elements, such as V, Cr, Ni, Co, U, Th, and Mo, are quite sensitive to changes in redox conditions; therefore, they are usually selected to characterize such conditions [7,29,30]. The concentration of U and Mo increase under anoxic conditions; thus, the content of U and Mo elements can indicate a redox environment [31].

Shale samples from the study area show quite substantial U and Mo enrichment, as the enrichment factor (EF) is generally much higher than 1 [15]. The average of U_{EF} is 3.51, with a range of 0.72 to 22.83. Mo is more enriched than U. Mo_{EF} ranges from 3.90 to 163.96, with an average of 25.61. This indicates that the shale samples in the study area are generally in a reducing environment (Figure 5, Table 3).

U_{EF} and Mo_{EF} show similar patterns of variation, with a gradually decrease from WF-F to U-LMX-F. The average U_{EF} in WF-F, L-LMX-F, M-LMX-F, and U-LMX-F is 9.15, 3.56,

2.64, and 1.38, respectively. The average Mo_{EF} in the four units is 79.19, 25.69, 13.64, and 9.00, respectively (Table 3), indicating the reduction intensity gradually weakens upward (Figure 5).

A covariation of Mo_{EF} - U_{EF} elements has been widely employed to explain redox conditions and restricted degrees of water mass. Shale samples in the study area are characterized by high values of Mo_{EF} , U_{EF} , and Mo_{EF}/U_{EF} , with Mo_{EF}/U_{EF} is mainly concentrated in $(1-3) \times SW$, which is higher than that in the Pengshui area of the Sichuan Basin [7]. The pattern of U–Mo covariation suggests that the Wufeng and Longmaxi Formation shale in Well Z303 was formed under dyoxic to anoxic conditions (Figure 7).

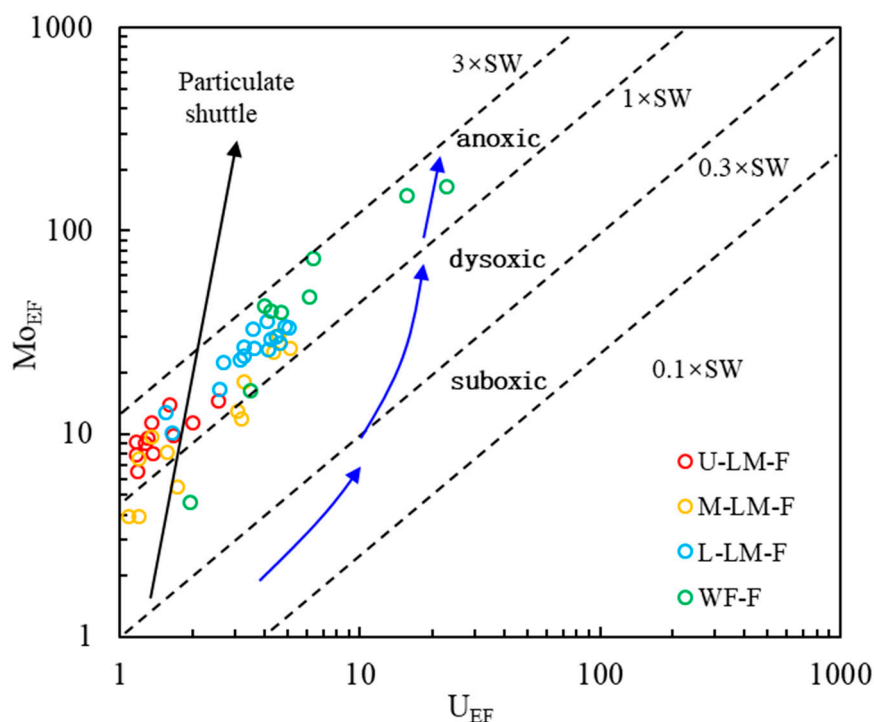


Figure 7. Cross plot of Mo_{EF} and U_{EF} in Well Z303, modified after [32]. SW is the molar ratio of Mo_{EF}/U_{EF} ; $1 \times SW$ is equal to the seawater value; $0.1 \times SW$, $0.3 \times SW$, and $3 \times SW$ are fractions (times) of SW; the SW value increases as the reduction conditions become stronger.

5.1.4. Paleoproductivity

P (phosphorus) and Cu (copper) are two key nutrient elements, playing an important role in promoting the growth of organisms in water. Thus, the two trace elements are essential proxies for primary productivity reconstruction [33–35]. The use of P and Cu as representatives of primary productivity needs to take into account the impact of terrestrial influx. Generally, Ti is a terrigenous sensitive element; thus, we take P/Ti and Cu/Ti ratios as the indicators of paleoproductivity characterization.

The P/Ti ratios generally witness a declining trend upward, range from 0.12 to 0.30 (average: 0.15), which are higher than that of PASS (average: 0.13), presenting a relatively high primary productivity (Figure 5). Shale samples in WF-F have the highest P/Ti ratio (avg. 0.20), followed by L-LMX-F (avg. 0.14), M-LMX-F (avg. 0.14), and U-LMX-F (avg. 0.13). Similar P/Ti ratio variations were also observed in Longmaxi Formation shale in the Pengshui area of the Sichuan Basin (P/Ti ratio avg. 0.105) [7]. The P/Ti ratio in the study area is higher than that of Pengshui area, indicating a higher paleoproductivity.

As is shown in Figure 8, the Cu/Ti ratios present a similar variation to the P/Ti ratios. The WF-F shale samples have the highest Cu/Ti ratios (0.015–0.05, avg. 0.024); Cu/Ti ratios during LMX-F are relatively low (avg. 0.014, 0.015, 0.016).

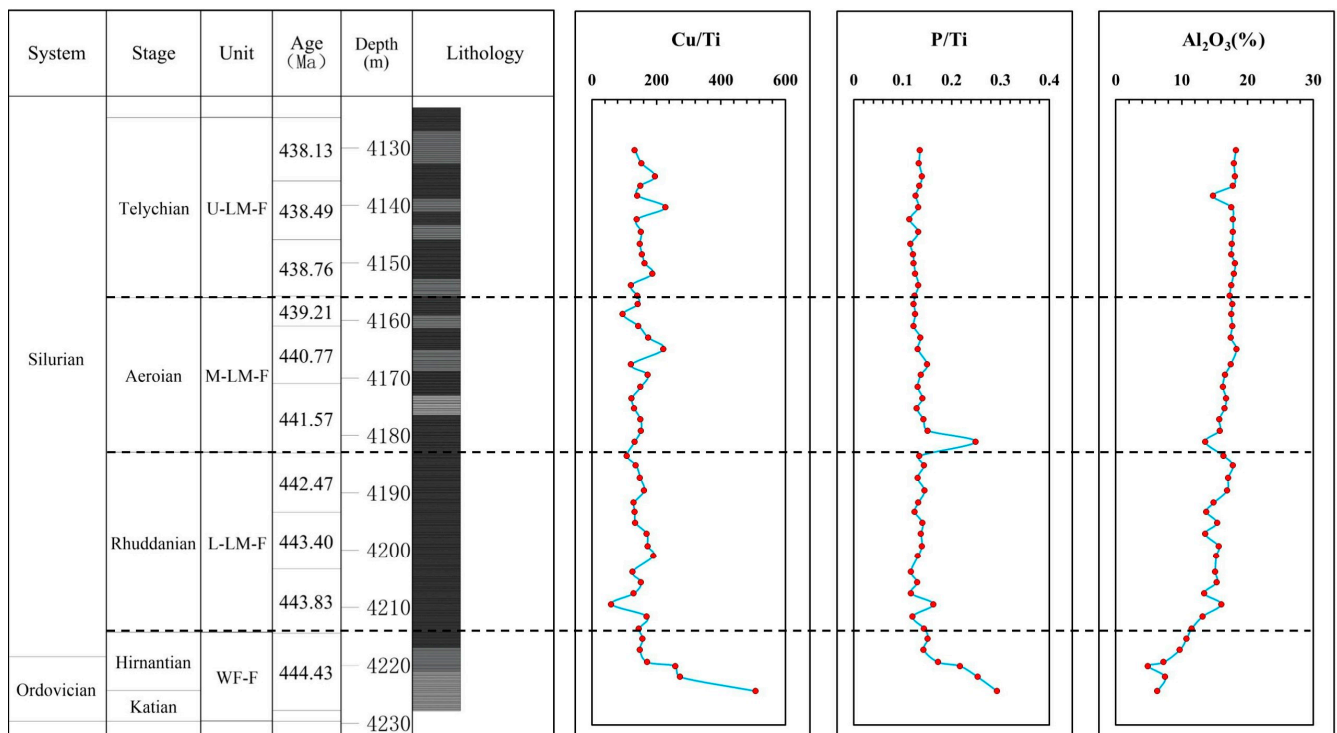


Figure 8. Variations of TOC, Cu/Ti, P/Ti, and Al₂O₃ in Well Z303.

5.1.5. Terrigenous Influx

Al₂O₃ has been widely used to indicate terrigenous detrital input in previous studies [36]. In the studied Al₂O₃ profile of Well Z303, Al₂O₃ exhibits a long-term increasing trend (Figure 9). The average Al₂O₃ in WF-F, L-LMX-F, M-LMX-F, and U-LMX-F is 8.29%, 15.22%, 17.00%, and 17.61%, respectively (Table 3). The Al₂O₃ content in WF-F and L-LMX-F is obviously less than that in M-LMX-F and U-LMX-F, indicating a sudden increase in terrigenous supply during the transition of Aeroian to Rhuddanian (Figures 1D and 7).

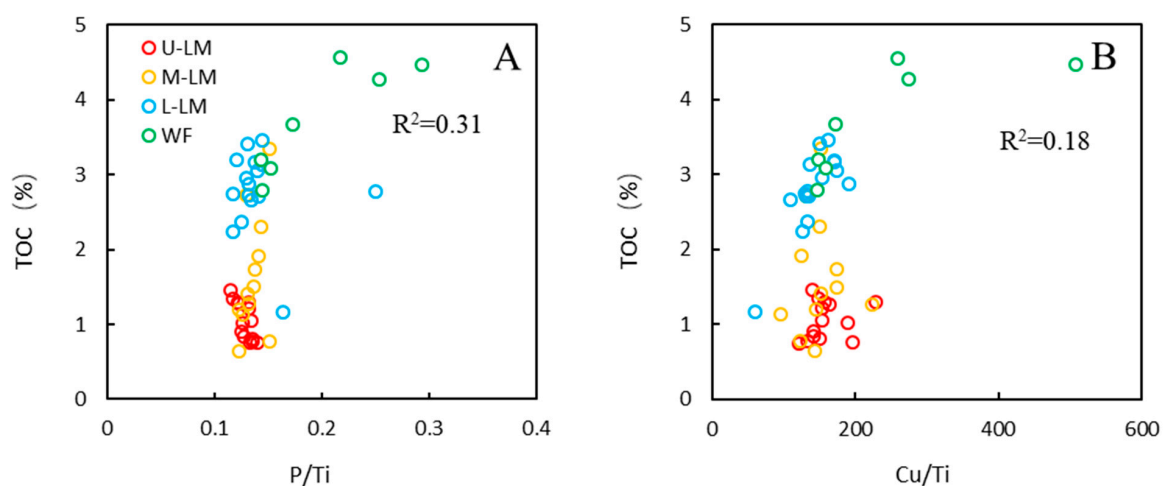


Figure 9. Cont.

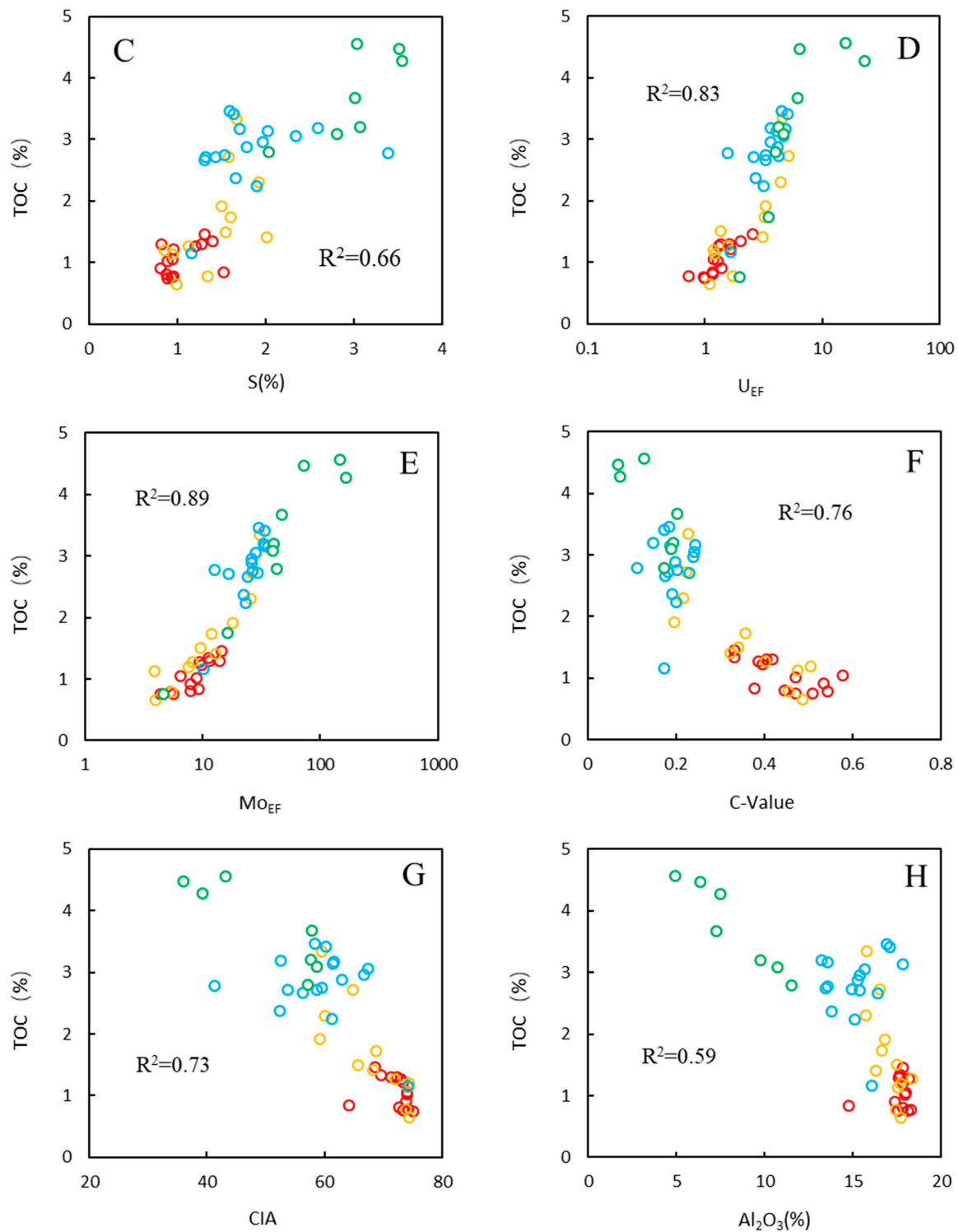


Figure 9. Correlations between TOC and P/Ti, Cu/Ti, C-value, CIA, Sr/Ba, U_{EF} , Mo_{EF} , and Al_2O_3 in Well Z303. (A) TOC vs. P/Ti; (B) TOC vs. Cu/Ti; (C) TOC vs. S; (D) TOC vs. U_{EF} ; (E) TOC vs. Mo_{EF} ; (F) TOC vs. C-Value; (G) TOC vs. CIA; (H) TOC vs. Al_2O_3 .

5.2. The Effect of Depositional Environment on OM Accumulation

Previous studies have shown that the enrichment of OM is generally controlled by three main factors: high primary productivity, anoxic reducing conditions, and low terrigenous influx [7,8,14,37].

By conducting correlation analysis between various sedimentary environmental parameters and TOC, the main controlling factors for organic matter enrichment can be determined (Figure 9). Correlation analysis results show that TOC contents demonstrate positive correlations with P/Ti and Cu/Ti (Figure 9A,B), but the correlation coefficient R^2 between P/Ti, Cu/Ti, and TOC is only 0.31 and 0.18, respectively; this indicates that the high level of paleoproductivity has a certain promoting effect on the formation of organic matter-rich shale in the study area, but it is not the main controlling factor. The paleosalinity parameter S element has a positive correlation with TOC (Figure 9C, $R^2 = 0.66$), and the redox parameters U_{EF} and Mo_{EF} have a strong positive correlation with TOC (Figure 9D,E, $R^2 = 0.83$ and 0.89 , respectively), indicating that the saline water reduction environment provides superior preservation conditions for organic matter enrichment and is the main controlling factor for organic matter enrichment in the study area. In addition, there is a significant positive correlation between the paleoclimate parameters C-value and chemical weathering index CIA and TOC (Figure 9F,G, $R^2 = 0.76$ and 0.73 , respectively); the terrigenous influx parameter Al_2O_3 also has a significant negative correlation with TOC (Figure 9H, $R^2 = 0.59$), indicating that paleoclimate, chemical weathering, and terrigenous influx also affect the formation of organic matter-rich shale in the study area.

The accompanying data help illustrate the effect of depositional environment on OM accumulation. The paleoclimate controlled the ancient ocean hydrologic conditions, including chemical weathering conditions, salinity, redox conditions, and terrigenous influx. Correlation analysis shows that C-value has a significant positive correlation with CIA (Figure 10A, $R^2 = 0.72$), indicating that paleoclimate controls the intensity of chemical weathering conditions. This phenomenon is due to hot and arid paleoclimate conditions corresponding to a weak weathering condition, while warm and humid paleoclimate conditions correspond to a strong weathering condition. There is a strong negative correlation between CIA and S (Figure 10B, $R^2 = 0.71$). This shows that paleoclimate has a significant impact on paleosalinity. This can be explained by the fact that, under an arid paleoclimate, the evaporation intensity is strong, and the freshwater recharge is usually restricted; thus, the water salinity increases. When the paleoclimate becomes warm and wet, the evaporation intensity decreases, and the fresh water input increases, leading to the reduction of water salinity. An appropriate increase in salinity is also beneficial for enhancing water stratification and providing a superior reducing environment for OM enrichment. In addition, positive correlation between CIA and Al_2O_3 value (Figure 10C, $R^2 = 0.64$) suggests that strong chemical weathering conditions have significant control over the terrigenous influx.

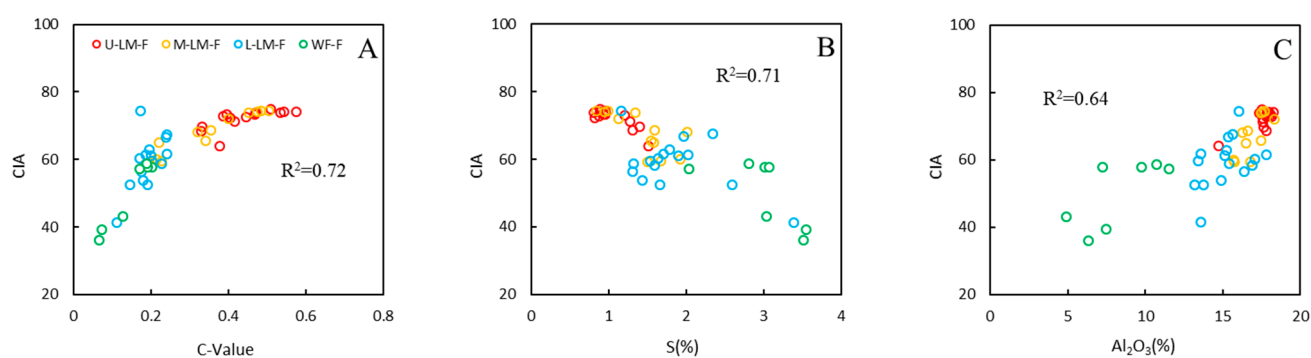


Figure 10. Correlations between CIA and C-value, Sr/Ba, and Al_2O_3 in Well Z303. (A): CIA vs. C-value; (B): CIA vs. Sr/Ba; (C): CIA vs. Al_2O_3 .

6. Conclusions

- (1) The Wufeng and Longmaxi Formations in the Zigong area represent high-quality source rock containing type I kerogen; the thermal evolution of the organic matter

is in late mature stage. The mineral compositions are dominated by quartz and clay minerals, with subordinated dolomite, feldspar, calcite, and pyrite.

- (2) Paleoenvironment indicators suggest that during the sedimentary period of Hirnantian and Rhuddanian, the paleoclimate condition was humid, the weathering condition was weak, anoxic conditions were present, and there was a high paleoproductivity and a low terrigenous detritus influx. During the period of Rhuddanian-Aeroian, the climate became drier and hotter, the intensity of weathering conditions became stronger, redox conditions were relatively reduced, terrigenous detritus influx increased, and paleoproductivity decreased.
- (3) The redox conditions were the most critical factor controlling the enrichment of OM. A combination of anoxic bottom water conditions with high primary productivity and low terrigenous input resulted in the greatest enrichment of organic matter in WF-F and L-LMX-F, making this a potential exploration and development target.

Author Contributions: Data curation, methodology and visualization, H.L.; funding acquisition, T.H. and W.L. All authors have read and agreed to the published version of the manuscript.

Funding: The authors are grateful for the support from the open fund of the State Center for Research and Development of Oil Shale Exploitation (33550007-22-ZC0613-0040) and the National Natural Science Foundation of China (41872118).

Institutional Review Board Statement: Not applicable.

Informed Consent Statement: Not applicable.

Data Availability Statement: Data are available from the authors upon request.

Acknowledgments: The authors would like to express their gratitude to the Hailong Wang from the PetroChina Jilin Oilfield Company for providing the background information required in this study. We also acknowledge the valuable feedback of the editors and reviewers.

Conflicts of Interest: The authors declare no conflict of interest.

References

1. Liu, Z.; Yan, D.; Yuan, D. Multiple controls on the organic matter accumulation in early Cambrian marine black shales, middle Yangtze Block, South China. *J. Nat. Gas Sci. Eng.* **2022**, *100*, 104454. [[CrossRef](#)]
2. Tang, L.; Song, Y.; Jiang, S.; Jiang, Z.; Li, Z.; Yang, Y.; Li, X.; Xiao, L. Organic matter accumulation of the Wufeng-Longmaxi shales in southern Sichuan Basin: Evidence and insight from volcanism. *Mar. Petrol. Geol.* **2020**, *120*, 104564. [[CrossRef](#)]
3. Zhang, L.; Li, B.; Shu, J. Heterogeneity characterization of the lower Silurian Longmaxi marine shale in the Pengshui area, South China. *Int. J. Coal Geol.* **2018**, *195*, 250–266. [[CrossRef](#)]
4. Hu, Z.; Li, W.; Zhang, H. Mg isotope evidence for restriction events within the Paleotethys ocean around the Permian-Triassic transition. *Earth Planet Sci. Lett.* **2021**, *556*, 116704. [[CrossRef](#)]
5. Lüning, S.; Craig, B.; Loydell, K. Lower Silurian ‘hot shales’ in North Africa and Arabia: Regional distribution and depositional model. *Earth Sci. Rev.* **2000**, *49*, 121–200. [[CrossRef](#)]
6. Zou, C.; Dong, D.; Wang, Y.; Li, X.; Huang, J.; Wang, S.; Guan, Q.; Zhang, C.; Wang, H.; Honglin, L.; et al. Shale gas in China: Characteristics, challenges and prospects (II). *Pet. Explor. Dev.* **2015**, *43*, 182–196. [[CrossRef](#)]
7. Zhang, L.; Xiao, D.; Lu, S. Effect of sedimentary environment on the formation of organic-rich marine shale: Insights from major/trace elements and shale composition. *Int. J. Coal Geol.* **2019**, *204*, 34–50. [[CrossRef](#)]
8. Demaison, G.J.; Moore, G.T. Anoxic environments and oil source bed genesis. *AAPG Bull.* **1980**, *64*, 1179–1209. [[CrossRef](#)]
9. Arthur, M.A.; Dean, W.E.; Laarkamp, K.J.C.G. Organic carbon accumulation and preservation in surface sediments on the Peru margin. *Chem. Geol.* **1998**, *152*, 273–286. [[CrossRef](#)]
10. Mort, H.; Jacquat, O.; Adatte, T.; Steinmann, P.; Föllmi, K.; Matera, V.; Berner, Z.; Stüben, D. The Cenomanian/Turonian anoxic event at the Bonarelli Level in Italy and Spain: Enhanced productivity and/or better preservation? *Cretac. Res.* **2007**, *28*, 597–612. [[CrossRef](#)]
11. Li, Y.; Zhang, T.; Ellis, G.S.; Shao, D. Depositional environment and organic matter accumulation of Upper Ordovician-Lower Silurian marine shale in the Upper Yangtze Platform, South China. *Palaeogeogr. Palaeoclimatol. Palaeoecol.* **2017**, *466*, 252–264. [[CrossRef](#)]
12. Pedersen, T.F.; Calvert, S.E.J.A.B. Anoxia vs. productivity: What controls the formation of organic- carbon-rich sediments and sedimentary rocks? *AAPG Bull.* **1990**, *74*, 454–466.
13. Liang, D.; Guo, T.; Chen, J. Some Progresses on Studies of Hydrocarbon Generation and Accumulation in Marine Sedimentary Regions, Southern China(Part 1): Distribution of Four Suits of Regional Marine Source Rocks. *Mar. Orig. Pet. Geol.* **2008**, *13*, 1–16.

14. Cai, Q.; Hu, M.; Kane, O.I. Cyclic variations in paleoenvironment and organic matter accumulation of the Upper Ordovician–Lower Silurian black shale in the Middle Yangtze Region, South China: Implications for tectonic setting, paleoclimate, and sea-level change. *Mar. Petrol. Geol.* **2022**, *136*, 105477. [[CrossRef](#)]
15. Taylor, S.R.; McLennan, S.M. The continental crust: Its composition and evolution. *Geol. J.* **1986**, *21*, 85–86.
16. Xia, L.; Cao, J.; Hu, S.; Li, S.; Shi, C. Organic geochemistry, petrology, and conventional and unconventional hydrocarbon resource potential of Paleogene saline source rocks in eastern China: The Biyang Sag of the Nanxiang Basin. *Mar. Petrol. Geol.* **2019**, *101*, 343–354. [[CrossRef](#)]
17. Wu, Y.; Lu, Y.; Jiang, S. Pore structure characterization of different lithofacies in marine shale: A case study of the Upper Ordovician Wufeng–Lower Silurian Longmaxi formation in the Sichuan Basin, SW China. *J. Nat. Gas Sci. Eng.* **2018**, *57*, 203–215. [[CrossRef](#)]
18. Armstrong-Altrin, J.S.; Yong, I.L.; Kasper-Zubillaga, J.J. Mineralogy and geochemistry of sands along the Manzanillo and El Carrizal beach areas, southern Mexico: Implications for palaeoweathering, provenance and tectonic setting. *Geological J.* **2017**, *52*, 559–582. [[CrossRef](#)]
19. Liu, B.; Song, Y.; Zhu, K. Mineralogy and element geochemistry of salinized lacustrine organic-rich shale in the Middle Permian Santanghu Basin: Implications for paleoenvironment, provenance, tectonic setting and shale oil potential. *Mar. Petrol. Geol.* **2020**, *120*, 104569. [[CrossRef](#)]
20. Getaneh, W. Geochemistry provenance and depositional tectonic setting of the Adigrat Sandstone northern Ethiopia. *J. Afr. Earth Sci.* **2002**, *35*, 185–198. [[CrossRef](#)]
21. Zhao, Z.Y.; Zhao, J.H.; Wang, H.J.; Liao, J.D.; Liu, C.M. Distribution characteristics and applications of trace elements in junggar basin. *Natural Gas Explor. Dev.* **2007**, *30*, 30–32.
22. Tan, Z.; Lu, S.; Li, W.; Zhang, Y.; He, T.; Jia, W.; Peng, P. Climate-driven variations in the depositional environment and organic matter accumulation of lacustrine mudstones: Evidence from organic and inorganic geochemistry in the Biyang Depression, Nanxiang Basin, China. *Energy Fuels* **2019**, *33*, 6946–6960. [[CrossRef](#)]
23. Nesbitt, H.; Young, G. Early Proterozoic climates and plate motions inferred from major element chemistry of lutites. *Nature* **1982**, *299*, 715–717. [[CrossRef](#)]
24. Hu, T.; Pang, X.; Jiang, S.; Wang, Q.; Xu, T.; Lu, K.; Huang, C.; Chen, Y.; Zheng, X. Impact of Paleosalinity, Dilution, Redox, and Paleoproductivity on Organic Matter Enrichment in a Saline Lacustrine Rift Basin: A Case Study of Paleogene Organic-Rich Shale in Dongpu Depression, Bohai Bay Basin, Eastern China. *Energy Fuels* **2018**, *32*, 5045–5061. [[CrossRef](#)]
25. Qian, L.J.; Chen, H.D.; Lin, L.B.; Xu, S.L.; Ou, L.H. Geochemical Characteristics and Environmental Implications of Middle Jurassic Shaximiao Formation, Western Margin of Sichuan Basin. *Acta Sedimentol. Sin.* **2012**, *30*, 1061–1071.
26. Wang, X.; Li, J.; Huang, Y.; Lu, S.; Chen, K.; Wei, Y.; Song, Z.; Zhao, R.; He, T. Influence of Paleosedimentary Environment on Shale Oil Enrichment in the Raoyang Sag, Bohai Bay Basin. *Energy Fuels* **2022**, *36*, 13597–13616. [[CrossRef](#)]
27. He, T.; Lu, S.; Li, W.; Tan, Z.; Zhang, X. Effect of Salinity on Source Rock Formation and Its Control on the Oil Content in Shales in the Hetaoyuan Formation from the Biyang Depression, Nanxiang Basin, Central China. *Energy Fuels* **2018**, *32*, 6698–6707. [[CrossRef](#)]
28. Li, D.; Li, R.; Zhu, Z.; Wu, X.; Cheng, J.; Liu, F.; Zhao, B. Origin of organic matter and paleo-sedimentary environment reconstruction of the Triassic oil shale in Tongchuan City, southern Ordos Basin (China). *Fuel* **2017**, *208*, 223–235. [[CrossRef](#)]
29. Jones, B.; Manning, D.A. Comparison of geochemical indices used for the interpretation of palaeoredox conditions in ancient mudstones. *Chem. Geol.* **1994**, *111*, 111–129. [[CrossRef](#)]
30. Tribovillard, N.; Algeo, T.J.; Lyons, T. Trace metals as paleoredox and paleoproductivity proxies: An update. *Chem. Geol.* **2006**, *232*, 12–32. [[CrossRef](#)]
31. Algeo, T.J.; Tribovillard, N. Environmental Analysis of Paleooceanographic Systems Based on Molybdenum–Uranium Covariation. *Chem. Geol.* **2009**, *268*, 211–225. [[CrossRef](#)]
32. Li, N.; Li, C.; Algeo, T.J.; Cheng, M.; Jin, C.; Zhu, G.; Fan, J.; Sun, Z. Redox changes in the outer Yangtze Sea (South China) through the Hirnantian Glaciation and their implications for the end-Ordovician biocrisis. *Earth Sci. Rev.* **2021**, *212*, 103443. [[CrossRef](#)]
33. Goldberg, E.D.; Arrhenius, G.O.S. Chemistry of Pacific pelagic sediments. *Geochim. Cosmochim. Ac.* **1958**, *13*, 153–212. [[CrossRef](#)]
34. Jack, D.; Erwin, S.; Mitch, L. Barium in Deep-Sea Sediment: A Geochemical Proxy for Paleoproductivity. *Paleoceanography* **2010**, *7*, 163–181.
35. Robert, W. Nutrient Limitation of Net Primary Production in Marine Ecosystems. *Annu. Rev. Ecol. Syst.* **1988**, *19*, 89–110.
36. Murphy, A.E.; Sageman, B.B.; Hollander, D.J.; Lyons, T.W.; Brett, C.E. Black shale deposition and faunal overturn in the Devonian Appalachian Basin: Clastic starvation, seasonal water-column mixing, and efficient biolimiting nutrient recycling. *Paleoceanography* **2000**, *15*, 280–291. [[CrossRef](#)]
37. Hao, F.; Tian, J.; Xu, Q. Paleoenvironment evolution of the lacustrine organic-rich shales in the second member of Kongdian Formation of Cangdong Sag, Bohai Bay Basin, China: Implications for organic matter accumulation. *Mar. Petrol. Geol.* **2021**, *133*, 105244.

Disclaimer/Publisher’s Note: The statements, opinions and data contained in all publications are solely those of the individual author(s) and contributor(s) and not of MDPI and/or the editor(s). MDPI and/or the editor(s) disclaim responsibility for any injury to people or property resulting from any ideas, methods, instructions or products referred to in the content.